TECHNISCHE MECHANIK, 33, 1, (2013), 19 – 33
submitted: July 19, 2012

On the Elastic Modeling of Highly Extensible Polyurea

T. Reppel, T. Dally, K. Weinberg

Polyurea is a soft and highly flexible material commonly used as protective coating on concrete or steel structures. Often subjected to abrasion and impact loading, numerical simulations of such structures require material models accounting for both stiffness and high extensibility of the coating. Hence, comparing several classical approaches with emphasis on efficiency and material stability, for impact simulations a Mooney-Rivlin model with $\mu_1 = 6$ MPa and $\mu_2 = 1.5$ MPa is suggested. Therefor material parameters from different sources are collected and, additionally, data from our uniaxial tension experiments are provided. The modeling is verified by comparison with a Taylor anvil impact experiment.

1 Introduction

Engineering materials generally need a certain strength and stiffness in order to carry loads and to provide structural properties. Soft and extensible polymers, however, are typically used as protective coatings and liners. Such a high performance elastomer of growing importance is polyurea, a flexible aminoplast with structural formula $[-\mathrm{NH}-(\mathrm{C{=}O})-\mathrm{NH}-\mathrm{R}^*-]_n$; different residual groups R^* are possible. Polyurea coatings combine strength with extensibility; the material is highly resistant and known to mitigate abrasive wear and destruction.

From their typical application as a protective coating of concrete and steel structures follows that elastomeric coatings have to withstand not only abrasion but also rapid loadings like impacts, collisions or explosions. Therefore we aim to model the material behavior of polyurea in the static as well as in the dynamic loading regime. Even under such extreme conditions polyurea often deforms in a reversible way and may thus be considered an elastic material. This, in turn, raises the question of how to model the elastic response. Here we do not aim at developing new hyperelastic material models - this would be redundant regarding the bulk of literature on this topic - but discuss the existing models and their suitability for modeling soft, highly extensible polymers in a mathematical stable and numerical efficient way. Exemplarily we study a Taylor anvil impact test where a cylindrical specimen hits a rigid surface with defined velocity, see Fig. 1 for an illustration of the experiment. A comparison of the specimen's deformation with numerical simulations provides useful information to validate the material constitutive constants.

The paper is organized as follows: In Section 2 we collect material data for polyurea including our own

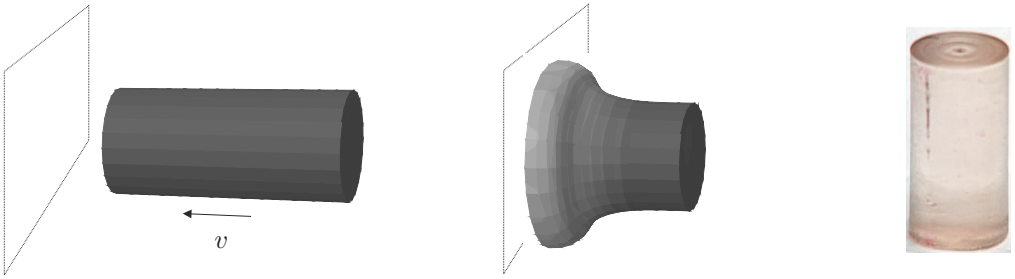

Figure 1: Schematic of an Taylor anvil impact experiment before and at impact (left and middle) and a polyurea specimen recovered after impact with $v = 254$ m/s (right); Reina (2010)

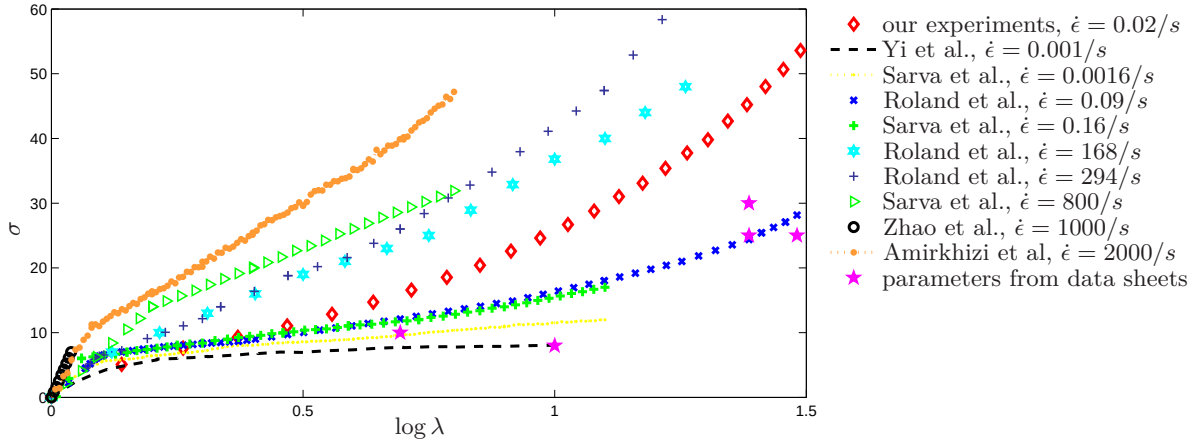

Figure 2: Cauchy stress σ versus true strain $\epsilon = \log \lambda$ for polyurea at different true strain rates $\dot{\epsilon}$; data collected from (Roland et al., 2007; Sarva et al., 2007; Yi et al., 2006; Zhao et al., 2007; Amirkhizi et al., 2006) with parameters from data sheets of commercial polyurea suppliers and our uniaxial tension test data added

uniaxial tension test measurements in order to summarize the basic properties of polyurea in quasistatic and dynamic straining. In Section 3 the classical elastic material models are presented and employed to simple stress states of an incompressible solid. Their suitability for describing materials undergoing large elongations will then be discussed with particular emphasis on stability. In Section 4 numerical results on the Taylor anvil impact test are presented and compared to experimental data.

2 Material Data

Polyurea, a one-step reaction product of an isocyanate and a resin blend component, is a rubbery material with high tensile strength and elongation up to 500-700%. Several tension and compression experiments of polyurea are reported in the literature, however, only few of them are comprehensive. Fig. 2 collects the corresponding stress-strain curves for the quasistatic and the dynamic regime in the range of interest. The quasistatic data are obtained in classical uniaxial tension setups whereas most of the dynamic data are deduced from uniaxial compression using Split-Hopkinson Bar tests, cf. Amirkhizi et al. (2006); Chakkarapani et al. (2006); Roland et al. (2007); Tekalur et al. (2008); Yi et al. (2006); Sarva et al. (2007); Zhao et al. (2007). The rate of straining influences the material's response appreciably. Knauss and Zhao (2007); Zhao et al. (2007) investigated the rate dependence of polyurea at small deformations in order to deduce viscoelastic material data. Sarva et al. (2007) reported large deformation stress-strain curves in compression for strain rates ranging from 0.001 s^{-1} to 9000 s^{-1}. The data of Roland et al. (2007) are obtained over a wide range of strain rates in uniaxial tension and converted into true (logarithmic) strain here. Additionally the authors contribute data from our quasistatic uniaxial tension tests (red diamonds in Fig. 2). Here, flat strips with initial length of $L_0 = 32$ mm and width of $B_0 = 10$ mm were pulled until 650% of straining, cf. Figure 3.

Clearly, the experimental data from different setups are not always in good agreement but they all show the same tendency. After a relatively stiff onset of straining all stress-strain curves show a decaying slope up to elongations of 4-5, only then followed by some strain stiffening. This is most obvious in the quasistatic measurements but it can be observed at high strain rates as well. For example, Amirkhizi et al. (2006) report the instantaneous stiffness of the material to significantly reduce at around 8% strain even at strain rates of about $2000/s$. In other words, at the beginning the material appears to be stiff with a quasistatic elastic modulus of about 70 MPa (Knauss and Zhao (2007)) and even higher values for high strain rates. In the course of deformation, however, the material shows less resistance to further straining. This indicates certain damaging effects and/or plastic flow. The recovered parts, however, show a mostly elastic behavior of polyurea, cf. Fig. 1. Even strongly deformed specimen completely regained their shape. Thence, we will focus here on *elastic* models in order to capture the high extensibility of polyurea in numerical computations.

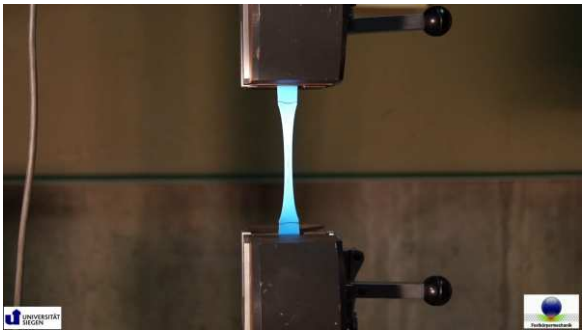

Figure 3: Uniaxial tension test of polyurea with feed of 2mm/s

3 Elastic Material Models

3.1 Preliminaries

Let $\boldsymbol{C} = \boldsymbol{F}^T\boldsymbol{F}$ and $\boldsymbol{B} = \boldsymbol{F}\boldsymbol{F}^T$ be the right and left Cauchy-Green tensor, respectively, with $\boldsymbol{F}$ being the deformation gradient. The material response derives from an elastic strain-energy density W^e. Moreover, elastomers are usually assumed to be elastically incompressible and so any admissible deformation is considered to be isochoric, i.e.:

$$\det(\boldsymbol{F}) = J = 1 \tag{1}$$

Accounting for this constraint we obtain $W^e = W(\boldsymbol{F}) - p(J-1)$, where $W(\boldsymbol{F})$ is the strain-energy density of the constitutive model and p is the hydrostatic pressure, here acting as a Lagrange multiplier. Taking the derivative with respect to the deformation gradient yields the first Piola-Kirchhoff stress tensor:

$$\boldsymbol{P} = \frac{\partial W^e}{\partial \boldsymbol{F}} = -pJ\boldsymbol{F}^{-T} + \frac{\partial W(\boldsymbol{F})}{\partial \boldsymbol{F}} \overset{(1)}{=} -p\boldsymbol{F}^{-T} + 2\boldsymbol{F}\frac{\partial W(\boldsymbol{C})}{\partial \boldsymbol{C}} \tag{2}$$

The Cauchy stress tensor $\boldsymbol{\sigma}$ follows by multiplication of (2) with $\boldsymbol{F}^T$ from the right.

$$\boldsymbol{\sigma} = -p\boldsymbol{I} + 2\boldsymbol{F}\frac{\partial W(\boldsymbol{C})}{\partial \boldsymbol{C}}\boldsymbol{F}^T \tag{3}$$

The mathematical treatment of the elastic problem typically seeks for a deformation minimizing the body's free energy subjected to specific boundary conditions. From calculus of variations it is well known that the existence of a minimizing (scalar) function can be guaranteed if the corresponding functional is convex. In higher dimensions it is necessary to weaken the condition of convexity to generalizations, namely quasiconvexity and polyconvexity, cf. Morrey (1966); Ball (1976). Whereas the first is an integral notion difficult to check or contradict, polyconvexity is a local property given if a tensorial function $W(\boldsymbol{A})$ can be written as a convex function of all subdeterminants of tensor $\boldsymbol{A}$. Specifically, an elastic strain energy density $W(\boldsymbol{F})$ is polyconvex if there exists a convex function $g : \mathbb{R}^{3\times3} \times \mathbb{R}^{3\times3} \times \mathbb{R} \to \mathbb{R}$ such that

$$W(\boldsymbol{F}) = g(\boldsymbol{F}, \mathrm{adj}\boldsymbol{F}, \det \boldsymbol{F}) \ . \tag{4}$$

In consequence, a way to guarantee the existence of a unique solution is to show polyconvexity of the corresponding elastic strain-energy density. Polyconvexity implies rank-one convexity of the elastic energy, which is equivalent to the Legendre-Hadamard condition of ellipticity. However, polyconvexity is not a necessary condition for ellipticity. In fact, simple empirical restrictions have been discussed in Bilgili (2004) for models of isotropic elasticity. In most cases such weaker conditions are sufficient for a well-posed elastic problem. Here we study different elastic material models in simple states of deformation, such as uni- and biaxial tension, simple and pure shearing. Simple deformation states can directly be compared to experimentally obtained data. From this the material model may be extrapolated to general deformations to be employed in statical and dynamical computations.

In order to ensure objectivity the elastic strain-energy density is to be formulated as a function of tensor $\boldsymbol{C}$. For isotropic material $W(\boldsymbol{C})$ can be expressed by the principle invariants I_a, $a = 1, 2, 3$ of the tensor,

$$I_1(\boldsymbol{C}) = \mathrm{tr}\boldsymbol{C} \qquad I_2(\boldsymbol{C}) = \frac{1}{2}\Big((\mathrm{tr}\boldsymbol{C})^2 - \mathrm{tr}(\boldsymbol{C}^2)\Big) \qquad I_3(\boldsymbol{C}) = \det \boldsymbol{C} \tag{5}$$

with $I_a(\boldsymbol{C}) = I_a(\boldsymbol{B})$. Please note, that the invariants directly correspond to the subdeterminant terms in condition (4). In particular, since $\mathrm{tr}\boldsymbol{C} = \mathrm{tr}\boldsymbol{F}^2$ we have $I_1 = |\boldsymbol{F}|^2$, i.e., I_1 relates to the deformation of a differential line element. From Cayley-Hamilton's theorem we also know $I_2(\boldsymbol{C}) = \mathrm{tr}(\mathrm{adj}\boldsymbol{C})$ and it follows $I_2 = |\mathrm{adj}\boldsymbol{F}|^2$, relating it to the deformation of a surface element. The relation of $I_3 = |\det \boldsymbol{F}|^2$ to the differential volume element is obvious.

Because constraint (1) corresponds to $\mathrm{I}_3 = 1$ the response of an isotropic incompressible elastic material will be determined by an strain-energy density being a function of the independent deformation variables I_1 and I_2. Using $p/2$ as a Lagrange multiplier we obtain:

$$W^e = W(I_1, I_2) - \frac{p}{2}(I_3 - 1) \tag{6}$$

Differentiating with respect to $\boldsymbol{C}$, where ${}^{\partial I_1}/_{\partial \boldsymbol{C}} = \boldsymbol{I}$, ${}^{\partial I_2}/_{\partial \boldsymbol{C}} = I_1\boldsymbol{I} - \boldsymbol{C}$, ${}^{\partial I_3}/_{\partial \boldsymbol{C}} = I_3\boldsymbol{C}^{-1}$ gives

$$2\frac{\partial W^e}{\partial \boldsymbol{C}} = 2\left(\frac{\partial W^e}{\partial I_1} + I_1\frac{\partial W^e}{\partial I_2}\right)\boldsymbol{I} - 2\frac{\partial W^e}{\partial I_2}\boldsymbol{C} - p\underbrace{I_3}_{=1}\boldsymbol{C}^{-1}$$

and by left multiplication with $\boldsymbol{F}$ we obtain the first Piola-Kirchhoff stress tensor for an incompressible material.

$$\boldsymbol{P} = -p\,\boldsymbol{F}^{-T} + 2\left(\frac{\partial W}{\partial I_1} + I_1\,\frac{\partial W}{\partial I_2}\right)\,\boldsymbol{F} - 2\frac{\partial W}{\partial I_2}\,\boldsymbol{B}\boldsymbol{F} \tag{7}$$

Pushing forward, $\boldsymbol{\sigma} = J^{-1}\boldsymbol{P}\boldsymbol{F}^T$, and applying Cayley-Hamilton's theorem gives the Cauchy stress in the commonly known form

$$\boldsymbol{\sigma} = -p\,\boldsymbol{I} + 2\left(\frac{\partial W}{\partial I_1} + I_1\,\frac{\partial W}{\partial I_2}\right)\,\boldsymbol{B} - 2\frac{\partial W}{\partial I_2}\,\boldsymbol{B}^2 = -\tilde{p}\,\boldsymbol{I} + 2\frac{\partial W}{\partial I_1}\,\boldsymbol{B} - 2\frac{\partial W}{\partial I_2}\,\boldsymbol{B}^{-1} \tag{8}$$

with pressure $\tilde{p} = p - 2I_2\frac{\partial W}{\partial I_2}$ to be determined from equilibrium.

3.2 Hyperelastic Models

The simplest constitutive model for isotropic elastic material, first mentioned in Treloar (1944), is given by the *Neo-Hookean* strain-energy density

$$W = \frac{\mu}{2}(I_1 - 3) \tag{9}$$

where μ denotes the initial shear modulus originally derived from a Gaussian statistical mechanics model. The stresses follow from (7) and (8), respectively.

$$\boldsymbol{P} = -p\,\boldsymbol{F}^{-T} + \mu\boldsymbol{F} \tag{10}$$

$$\boldsymbol{\sigma} = -p\,\boldsymbol{I} + \mu\boldsymbol{B} \tag{11}$$

Accounting additionally for the second invariant gives in its simplest form the *Mooney-Rivlin* strain-energy density (cf. Rivlin and Saunders (1951)),

$$W = \frac{\mu_1}{2}(I_1 - 3) + \frac{\mu_2}{2}(I_2 - 3) \tag{12}$$

with $\mu_1 + \mu_2 = \mu$ being the initial shear modulus, and stresses:

$$\boldsymbol{P} = -p\,\boldsymbol{F}^{-T} + \mu_1\boldsymbol{F} + \mu_2\big(I_1\boldsymbol{I} - \boldsymbol{B}\big)\boldsymbol{F} \tag{13}$$

$$\boldsymbol{\sigma} = -p\,\boldsymbol{I} + \mu_1\boldsymbol{B} - \mu_2\boldsymbol{B}^{-1} \tag{14}$$

While both classical models are useful in describing rubbery materials at moderate stretches, their predictions do not adequately map experimental data for other elastomers or for biological tissue. This motivated the derivation of numerous additional elastic models. Without discussing their physical background we will here enlist some of them.

The model of Gent (1996) presumes an elastic strain-energy density of the form

$$W = -\frac{\mu}{2} c_G \ln\left(1 - \frac{I_1 - 3}{c_G}\right) \tag{15}$$

and is basically a two-parameter generalized Neo-Hookean model; for $c_G \to \infty$ it corresponds to (9). Parameter c_G is introduced to account for the limited extensibility of rubbery materials and induces rapid strain stiffening for large stretches. Values of $c_G = 30 \ldots 100$ are common for rubber, whereas in other materials smaller values may be appropriate. The Cauchy stress tensor for the Gent model follows as:

$$\boldsymbol{\sigma} = -p\boldsymbol{I} + \frac{\mu c_G}{c_G + 3 - I_1}\boldsymbol{B} \tag{16}$$

Clearly, it must hold $I_1 < c_G + 3$ and thus, strain-energy density (15) is not polyconvex for arbitrary deformation gradients. However, this does not necessarily mean that the model should be ruled out. The corresponding lack of ellipticity at large deformations is physically correct, indicating the onset of rupture and failure by 'failing' to compute elastic solutions.

Whereas the Gent model is purely phenomenological, a similar model motivated by *van der Waals* ideal gas theory has earlier been derived by Kilian (1980, 1981):

$$W = -\mu c_e \ln\left(1 - \sqrt{\frac{I_1 - 3}{c_e}}\right) - \mu c_e \sqrt{\frac{I_1 - 3}{c_e}} \tag{17}$$

Here shear modulus μ and parameter c_e (chain extensibility) summarize material constants derived from ideal gas theory and its similarity to the molecular networks of rubber plus considerations on limited extensibility of polymer chains. The stresses are:

$$\boldsymbol{\sigma} = -p\boldsymbol{I} + \frac{\mu}{1 - \sqrt{\frac{I_1-3}{c_e}}}\boldsymbol{B} \;= -p\boldsymbol{I} + \frac{\mu\sqrt{c_e}}{\sqrt{c_e} - \sqrt{I_1 - 3}}\boldsymbol{B} \tag{18}$$

Comparing (16) with (18) gives $c_G^2 = c_e(I_1 - 3)$ and, again, for $I_1 \to c_e + 3$ the stresses have a singularity causing a rapid strain stiffening before failure.

An appropriate model for materials with strong strain stiffening is the *Fung* model (Fung (1967)) of biomechanics,

$$W = \frac{\mu}{2c_F}\Big(\exp\big(c_F(I_1 - 3)\big) - 1\Big) \tag{19}$$

with a constant $c_F > 0$. Taking the limit $c_F \to 0$ the Neo-Hookean (9) may be recovered. Here the stresses follow as:

$$\boldsymbol{\sigma} = -p\boldsymbol{I} + \mu \exp\big(c_F(I_1 - 3)\big)\boldsymbol{B} \tag{20}$$

Both, the Gent/van der Waals model as well as the Fung model can be extended by a weighted term of $(I_2 - 3)$ which gives in the corresponding limits the Mooney-Rivlin model (12).

A generalized elastic strain-energy density may be written in form:

$$W = \sum_{i=1}^{N}\sum_{j=1}^{M} c_{ij}\big(I_1 - 3\big)^i\big(I_2 - 3\big)^j \;. \tag{21}$$

Introduced in Rivlin and Saunders (1951) as general Rivlin model, formulation (21) allows for any combination of polynomial terms, though polyconvexity requires $c_{ij} = 0$ for $i = j$, cf. Hartmann and Neff (2003). The special case of $N = 3$, $M = 0$ is known as *Yeoh* model, cf. (Yeoh, 1996),

$$W = \frac{\mu}{2}\big(I_1 - 3\big) + \frac{\mu c_1}{4}\big(I_1 - 3\big)^2 + \frac{\mu c_2}{6}\big(I_1 - 3\big)^3 \tag{22}$$

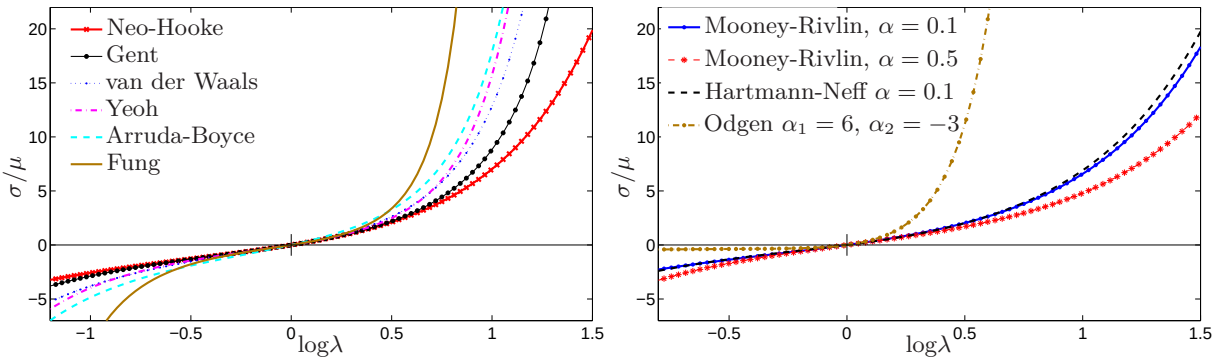

Figure 4: True stresses versus logarithmic strain $\epsilon = \log\lambda$ for different elastic materials compressed and elongated uniaxially. Left: all models are independent of the second invariant; material parameters used are $c_G = 25, c_e = 5$, $c_F = 0.5$, $c_1 = d_1 = 0.889$, $c_2 = d_2 = 0.0124$. Right: models with terms of the second invariant, $(1-\alpha)\mu_1 + \alpha\mu_2 = \mu$, and Ogden model with $N = 2$, $\alpha_1 = 6$, $\alpha_2 = -3$, $\mu_1 = 0.6\mu$, $\mu_2 = 0.56\mu$

with stresses:

$$\boldsymbol{\sigma} = -p\boldsymbol{I} + \mu\Big(1 + c_1\big(I_1 - 3\big) + c_2\big(I_1 - 3\big)^2\Big)\boldsymbol{B} \tag{23}$$

Many other combinations of polynomials are common. However, because most of these combinations do not result in polyconvex energy functions, a generalization like (21) is more of theoretical character.

Another class of energy functions in terms of only the first invariant has been introduced by Arruda and Boyce (1993), $W = \sum_{i=1}^{N} d_i(I_1^i - 3^i)$. The factors d_i are in part defined by a linearization of Langevin functions resulting from statistical treatments. For $N = 3$ we may write

$$W = \frac{\mu}{2}\big(I_1 - 3\big) + \frac{\mu d_1}{4}\big(I_1^2 - 9\big) + \frac{\mu d_2}{6}\big(I_1^3 - 27\big) \tag{24}$$

with stresses:

$$\boldsymbol{\sigma} = -p\boldsymbol{I} + \mu\Big(1 + d_1 I_1 + d_2 I_1^2\Big)\boldsymbol{B} \tag{25}$$

Here $d_1 = {}^1\!/_{5\lambda_c}$, $d_2 = {}^{11}\!/_{175\lambda_c^2}$, where material parameter λ_c describes a critical chain length. In Hartmann and Neff (2003) it was shown that function (24) is always polyconvex for $\lambda_c > 0$.

The left plot in Fig. 4 displays the stress-strain curves for different material models of the first invariant as a function of strain in uniaxial tension and compression. Models using the second invariant are mostly restricted to its first power, see Eq. (12). An alternative approach has been suggested by Hartmann and Neff (2003) using an exponent of 3/2.

$$W = \frac{\mu_1}{2}\big(I_1 - 3\big) + \frac{\mu_2}{3}\big(I_2 - 3\big)^{\frac{3}{2}} \tag{26}$$

The Cauchy stresses here follow as:

$$\boldsymbol{\sigma} = -p\boldsymbol{I} + \mu_1\boldsymbol{B} - \mu_2\big(I_2 - 3\big)^{\frac{1}{2}}\boldsymbol{B}^{-1} \tag{27}$$

Finally we state the general *Ogden* material model (Ogden, 1972) where the strain energy density is expressed in terms of the principal stretches $\lambda_a, a = 1, 2, 3$.

$$W = \sum_{p=1}^{N} \frac{\mu_p}{\alpha_p}\left(\lambda_1^{\alpha_p} + \lambda_2^{\alpha_p} + \lambda_3^{\alpha_p} - 3\right) \quad \text{with} \quad \sum_{p=1}^{N} \mu_p\alpha_p = 2\mu \tag{28}$$

Here μ is the initial shear modulus and μ_p, α_p are material constants. Polyconvexity requires

$$\mu_p\alpha_p > 0\ , \qquad |\alpha_p| > 1 \qquad \text{for all } p = 1, \ldots, N\ . \tag{29}$$

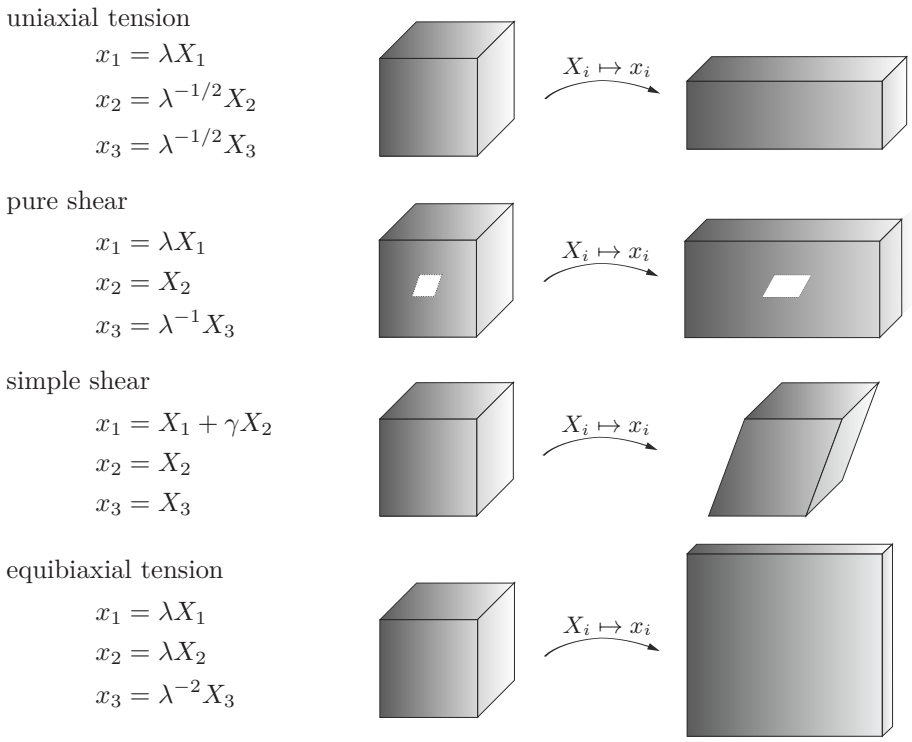

Table 1: Illustration of one- and two-dimensional states of deformation; capital letters denote the initial coordinates, lower case letters the current configuration.

The Neo-Hookean material and the Mooney-Rivlin material can be recovered from (28) by $N = 1, \alpha_1 = 2$ and $N = 2, \alpha_1 = 2, \alpha_2 = -2$, $\mu_2 < 0$, respectively. The stresses derive directly as principle stress components. This is convenient for simple states of deformation. For numerical computation however, constitutive models formulated in principal stretches require to solve eigenvalue problems in every step of solution at every material point. This renders the Ogden model an expensive alternative to models formulated in invariants.

For polyurea a two-parametric Ogden model with $\alpha_1 = 6$, $\alpha_2 = -3$ has been adapted to experimental data in Reina (2010), with the result $\mu_1 = 0.6\mu$, $\mu_2 = 0.56\mu$, see right plot in Fig. 4. With the material constants suggested, however, the model is unstable and not polyconvex and therefore we exclude it from further considerations.

A more comprehensive list of hyperelastic models can be found in Hoss and Marczak (2010). They also suggest a new set of elastic energy densities which are not restricted to be polyconvex. Unfortunately, no conditions are derived for a meaningful choice of the several introduced material constants, what makes it difficult to consider them for practical use.

3.3 Simple states of deformation

Material data are usually obtained using experimental settings with simple stress states described by the principle stretches, λ_a, $a = 1, 2, 3$. Then, the invariants of deformation (5) may as well be expressed by:

$$I_1 = \lambda_1^2 + \lambda_2^2 + \lambda_3^2 \ , \quad I_2 = \lambda_1^2\lambda_2^2 + \lambda_2^2\lambda_3^2 + \lambda_3^2\lambda_1^2 \ , \quad I_3 = \lambda_1^2\lambda_2^2\lambda_3^2 \tag{30}$$

and the elastic-strain energy is of the form $W^e = W(\lambda_1, \lambda_2, \lambda_3) - p\ (J-1)$ with $I_3 = J = 1$. The principle stress components of an incompressible material follow immediately from (7) and (8) as:

$$P_a = -\frac{p}{\lambda_a} + \frac{\partial W}{\partial \lambda_a} = -\frac{p}{\lambda_a} + \frac{\partial W}{\partial I_1}\frac{\partial I_1}{\partial \lambda_a} + \frac{\partial W}{\partial I_2}\frac{\partial I_2}{\partial \lambda_a}, \quad a = 1, 2, 3 \tag{31}$$

$$\sigma_a = -p + \lambda_a \frac{\partial W}{\partial \lambda_a} = P_a \lambda_a \tag{32}$$

Neo-Hookean material	$\sigma = \mu\left(\lambda^2 - \frac{1}{\lambda}\right)$
Mooney-Rivlin material	$\sigma = \mu_1\left(\lambda^2 - \frac{1}{\lambda}\right) + \mu_2\left(\lambda - \frac{1}{\lambda^2}\right)$
Gent material	$\sigma = \mu\left(\lambda^2 - \frac{1}{\lambda}\right)\frac{c_G}{c_G+3-I_1}$
van der Waals material	$\sigma = \mu\left(\lambda^2 - \frac{1}{\lambda}\right)\frac{\sqrt{c_e}}{\sqrt{c_e}-\sqrt{I_1-3}}$
Fung material	$\sigma = \mu\left(\lambda^2 - \frac{1}{\lambda}\right)\exp\left(c_F\left(I_1-3\right)\right)$
Yeoh material	$\sigma = \mu\left(\lambda^2 - \frac{1}{\lambda}\right)\left(1 + c_1\left(I_1-3\right) + c_2\left(I_1-3\right)^2\right)$
Arruda-Boyce material	$\sigma = \mu\left(\lambda^2 - \frac{1}{\lambda}\right)\left(1 + d_1 I_1 + d_2 I_1^2\right)$
Hartmann and Neff material	$\sigma = \mu_1\left(\lambda^2 - \frac{1}{\lambda}\right) + \mu_2\left(\lambda - \frac{1}{\lambda^2}\right)\sqrt{I_1-3}$
general Ogden material	$\sigma = \sum_{p=1}^{N} \mu_p\left(\lambda^{\alpha_p} - \lambda^{-\alpha_p/2}\right)$

Table 2: Cauchy stress in uniaxial tension, $I_1 = \lambda^2 + 2/\lambda$, $I_2 = 2\lambda + 1/\lambda^2$

Table 1 illustrates simple one- and two-dimensional states of deformation. From the constraint $\sigma_3 = 0$ the pressure evolves directly:

$$p = 2\lambda_3^2\frac{\partial W}{\partial I_1} + 2\lambda_3^2(\lambda_1^2+\lambda_2^2)\frac{\partial W}{\partial I_2} \overset{J=1}{=} \frac{2}{\lambda_1^2\lambda_2^2}\frac{\partial W}{\partial I_1} + \frac{2(\lambda_1^2+\lambda_2^2)}{\lambda_1^2\lambda_2^2}\frac{\partial W}{\partial I_2} \tag{33}$$

The classical **uniaxial tension** test presumes a state deformation with

$$\lambda_1 = \lambda \quad \text{and} \quad \lambda_2 = \lambda_3 = \frac{1}{\sqrt{\lambda}} \tag{34}$$

and, with $\sigma_2 = \sigma_3 = 0$ and (33), we may write for the uniaxial Cauchy stress $\sigma \equiv \sigma_1$

$$\sigma = 2\left(\lambda^2 - \frac{1}{\lambda}\right)\frac{\partial W}{\partial I_1} + 2\left(\lambda - \frac{1}{\lambda^2}\right)\frac{\partial W}{\partial I_2}\,. \tag{35}$$

Table 2 and Fig. 4 enlist the results for the different material models.

In an analogous manner we evaluate two-dimensional stress states with the principle Cauchy stress components

$$\sigma_1 = 2\left(\lambda_1^2 - \frac{1}{\lambda_1^2\lambda_2^2}\right)\frac{\partial W}{\partial I_1} + 2\left(\lambda_1^2\lambda_2^2 - \frac{1}{\lambda_1^2}\right)\frac{\partial W}{\partial I_2} \tag{36}$$

$$\sigma_2 = 2\left(\lambda_2^2 - \frac{1}{\lambda_1^2\lambda_2^2}\right)\frac{\partial W}{\partial I_1} + 2\left(\lambda_1^2\lambda_2^2 - \frac{1}{\lambda_2^2}\right)\frac{\partial W}{\partial I_2} \tag{37}$$

In the special case of

$$\lambda_1 = \lambda \quad , \quad \lambda_2 = 1 \quad \text{and} \quad \lambda_3 = \frac{1}{\lambda} \tag{38}$$

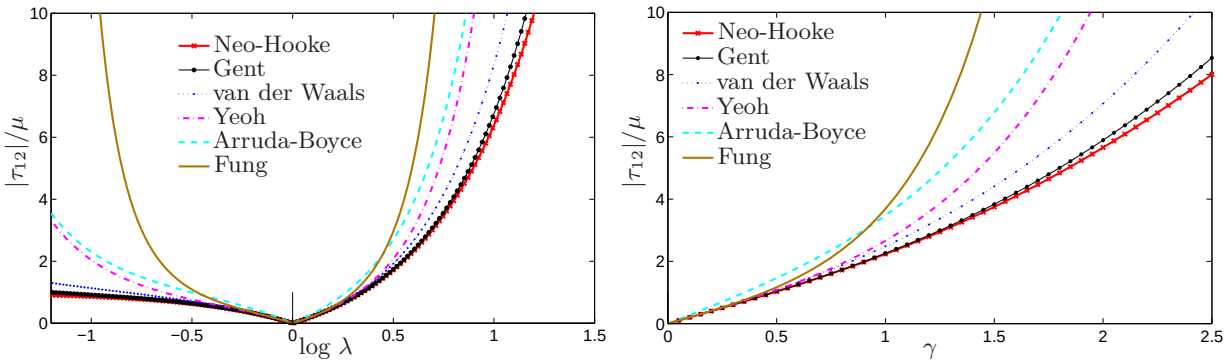

Figure 5: Absolut shear stress in pure shear (left) and simple shear (right) for different material models, parameters are $c_G = 25$, $c_F = 0.5$, $c_1 = d_1 = 0.889$, $c_2 = d_2 = 0.0124$.

	pure shear	simple shear
Neo-Hookean	$\tau = \mu\big(1-\lambda^2\big)$	$\tau = \mu\gamma\big(\gamma^2+4\big)^{1/2}$
Mooney-Rivlin	$\tau = \mu_1\big(1-\lambda^2\big) + \mu_2\big(\frac{1}{\lambda^2}-1\big)$	$\tau = \gamma(\mu_1+\mu_2)\big(\gamma^2+4\big)^{1/2}$
Gent	$\tau = \mu\big(1-\lambda^2\big)\frac{c_G}{c_G+3-I_1}$	$\tau = \mu\gamma\big(\gamma^2+4\big)^{1/2}\frac{c_G}{c_G+3-I_1}$
van der Waals	$\tau = \mu\big(1-\lambda^2\big)\frac{\sqrt{c_e}}{\sqrt{c_e}-\sqrt{I_1-3}}$	$\tau = \mu\big(\gamma^2+4\big)^{1/2}\frac{\sqrt{c_e}}{\sqrt{c_e}-\sqrt{I_1-3}}$
Fung	$\tau = \mu\big(1-\lambda^2\big)\exp\big(c_F(I_1-3)\big)$	$\tau = \mu\gamma\big(\gamma^2+4\big)^{1/2}\exp\Big(c_F\big(I_1-3\big)\Big)$
Yeoh	$\tau = \mu\big(1-\lambda^2\big)\big(1+c_1(I_1-3)+c_2(I_1-3)^2\big)$	$\tau = \mu\gamma\big(\gamma^2+4\big)^{1/2}\Big(1+c_1(I_1-3)+c_2(I_1-3)^2\Big)$
Arruda-Boyce	$\tau = \mu\big(1-\lambda^2\big)\Big(1+d_1I_1+d_2I_1^2\Big)$	$\tau = \mu\gamma\big(\gamma^2+4\big)^{1/2}\Big(1+d_1I_1+d_2I_1^2\Big)$
Hartmann-Neff	$\tau = \mu_1\big(1-\lambda^2\big) + \mu_2\big(\frac{1}{\lambda^2}-1\big)\sqrt{I_1-3}$	$\tau = \gamma(\mu_1+\mu_2\sqrt{I_1-3})\big(\gamma^2+4\big)^{1/2}$
general Ogden	$\tau = \sum_{p=1}^{N}\mu_p\big(\lambda^{\alpha_p}-1\big)$	$\tau = \sum_{p=1}^{N}\mu_p\left(\lambda_1^{\alpha_p}-\lambda_2^{\alpha_p}\right)$

Table 3: Shear stress in pure shear, $I_1 = I_2 = \lambda^2+\lambda^{-2}+1$ and in simple shear, $I_1 = I_2 = 3+\gamma^2$

we observe a biaxial tension state commonly known as **pure shear**. From (36-37) follows the principle shear stress:

$$\tau = \frac{1}{2}|\sigma_1-\sigma_2| = \big(1-\lambda^2\big)\,\frac{\partial W}{\partial I_1} + \left(\frac{1}{\lambda^2}-1\right)\frac{\partial W}{\partial I_2} \tag{39}$$

In a deformation state of **simple shear** the material is not elongated but sheared by an angle θ. With $\gamma = \tan(\theta)$ the eigenvalues λ_i^2 of the resulting right Cauchy-Green tensor are:

$$\lambda_1^2 = \frac{1}{2}\big(\gamma^2+2-\gamma\sqrt{\gamma^2+4}\big), \quad \lambda_2^2 = \frac{1}{2}\big(\gamma^2+2+\gamma\sqrt{\gamma^2+4}\big) \quad \lambda_3^2 = 1\ . \tag{40}$$

This directly evaluates to $I_1 = I_2 = 3+\gamma^2$ and $I_3 = 1$, i.e., the deformation is also isochoric. Evaluating the Cauchy stress components (36-37) we obtain the maximal shear stress,

$$\tau = \frac{1}{2}|\sigma_1-\sigma_2| = \gamma\sqrt{\gamma^2+4}\left(\frac{\partial W}{\partial I_1}+\frac{\partial W}{\partial I_2}\right)\ . \tag{41}$$

Tab. 3 summarizes the stresses for the different material models and Fig. 5 shows the maximal shear stresses as a function of deformation for both pure shear and simple shear states. Please note that in both cases $I_1 = I_2$ holds, and, thus there is no difference between Neo-Hookean and Mooney-Rivlin materials.

Finally we consider the case of **equibiaxial stretching**, i.e.,

$$\lambda_1 = \lambda_2 = \lambda \quad \text{and} \quad \lambda_3 = \frac{1}{\lambda^2} \tag{42}$$

Neo-Hookean material	$\sigma = \mu\big(\lambda^2-\frac{1}{\lambda^4}\big)$
Mooney-Rivlin material	$\sigma = \mu_1\big(\lambda^2-\frac{1}{\lambda^4}\big) + \mu_2\big(\lambda^4-\frac{1}{\lambda^2}\big)$
Gent material	$\sigma = \mu\big(\lambda^2-\frac{1}{\lambda^4}\big)\frac{c_G}{c_G+3-I_1}$
van der Waals material	$\sigma = \mu\big(\lambda^2-\frac{1}{\lambda^4}\big)\frac{\sqrt{c_e}}{\sqrt{c_e}-\sqrt{I_1-3}}$
Fung material	$\sigma = \mu\big(\lambda^2-\frac{1}{\lambda^4}\big)\exp\Big(c_F\big(I_1-3\big)\Big)$
Yeoh material	$\sigma = \mu\big(\lambda^2-\frac{1}{\lambda^4}\big)\Big(1+c_1\big(I_1-3\big)+c_2\big(I_1-3\big)^2\Big)$
Arruda-Boyce material	$\sigma = \mu\big(\lambda^2-\frac{1}{\lambda^4}\big)\Big(1+d_1I_1+d_2I_1^2\Big)$
Hartmann and Neff material	$\sigma = \mu_1\big(\lambda^2-\frac{1}{\lambda^4}\big) + \mu_2\big(\lambda^4-\frac{1}{\lambda^2}\big)\sqrt{I_1-3}$
general Ogden material	$\sigma = \sum_{p=1}^{N}\mu_p\left(\lambda^{\alpha_p}-\lambda^{-2\alpha_p}\right)$

Table 4: Cauchy stress in equibiaxial tension, $I_1 = 2\lambda^2+1/\lambda^4$, $I_2 = \lambda^4+2/\lambda^2$

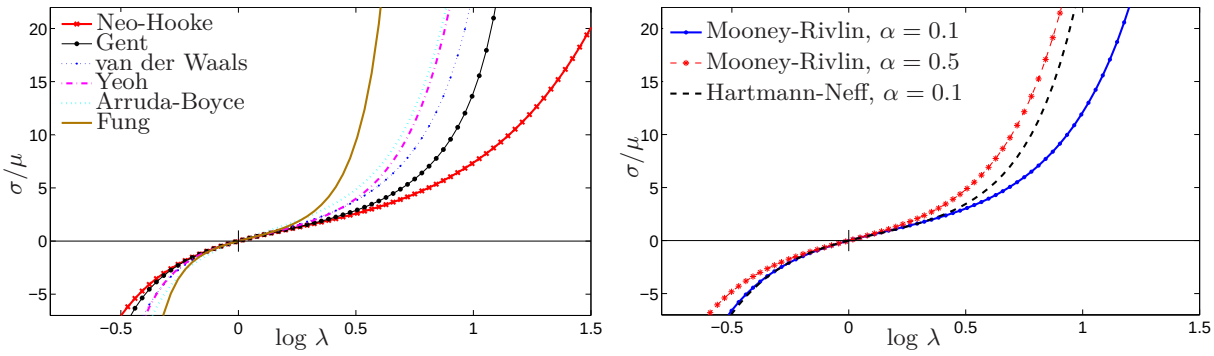

Figure 6: True stresses versus logarithmic strain $\epsilon = \log \lambda$ for different elastic materials compressed and elongated equibiaxially. Left: all models are independent of the second invariant; material parameters used are $c_G = 25, c_e = 5$, $c_F = 0.5$, $c_1 = d_1 = 0.889$, $c_2 = d_2 = 0.0124$. Right: Models with terms of the second invariant, $(1-\alpha)\mu_1 + \alpha\mu_2 = \mu$

and evaluate the in-plane stresses $\sigma = \sigma_1 = \sigma_2$ from (36-37), see Table 4.

$$\sigma = 2\left(\lambda^2 - \frac{1}{\lambda^4}\right)\frac{\partial W}{\partial I_1} + 2\left(\lambda^4 - \frac{1}{\lambda^2}\right)\frac{\partial W}{\partial I_2} \tag{43}$$

3.4 Discussion

In order to adapt the constitutive models to the experimental data we first study the stresses of different material models as a function of strain in uniaxial tension and compression, Fig. 4. All stress-strain curves are plotted in an admissible range of deformation, i.e., the corresponding energy densities $W(I_1, I_2)$ are polyconvex here; Gent and von der Waals model fail for higher straining. Clearly, for same initial shear moduli the Neo-Hookean model is bounding the stresses from below. This follows immediately from the fact that polynomial terms $(I_1 - 3)^i$ are convex only for $i \geq 1$ and the Neo-Hookean model is given by $i = 1$. Moreover, combinations of polynomial terms require positive material constants to guarantee polyconvexity of the resulting strain-energy functions, cf. Hartmann and Neff (2003). Although negative constants c_{1i} in (21) do not always result in a loss of polyconvexity, care needs to be take when applying such energy forms in numerical computations.

The Fung model (19) clearly shows the strongest strain stiffening, and, thus is not a model of choice for the application we have in mind. The Gent and van der Waals model have a singularity at $I_1 = c_G + 3$ and at $I_1 = c_e + 3$, respective, and the corresponding limiting stretch for well posedness can easily be calculated. For example, in uniaxial tension $c_G = 25$ corresponds to a failure of model (15) at $\lambda = 5.26$ whereas the same value in pure shear and equibiaxial tension gives material failure at $\lambda = 5.19$ and $\lambda = 3.74$; similar values hold for van der Waals model with $c_e = c_G$. Therefore, though the van der Waals model has a solid physical background, these models are not a proper choice for numerical computations.

The polynomial Yeoh model and the Arruda-Boyce model lead to a rising slope of the stress-strain curve. In the latter the material constants are positive by definition of the model. A polynomial form like (22) can be fitted to a specific set of stress-strain data. However, polyconvexity is only guaranteed for $c_i > 0$ in general. In particular, for a negative value of c_2 one can easily calculate the general convexity condition $c_1 > -2c_2(I_1 - 3)$. This reduces the rising slope only marginally. For example, with $c_2 = -0.1$ and $\lambda \in (0.25, 5)$ in uniaxial tension convexity is given for $c_1 > 4.48$ which corresponds to immediate strong stiffening and a minor reduction of stiffness later on.

A calibration of the material data using the general Ogden model may as well give a good agreement, see, e.g., El Sayed (2008); Reina (2010). However, the material characterization of El Sayed (2008); El Sayed et al. (2009) is cumbersome and very specific using different material models for different strain rates, whereas the fit of Reina (2010) holds only in the compressive range (loss of convexity for $\lambda > 1$, see comments in Section 2). In general, stable fits following restrictions (29) are very similar to the models discussed here and, moreover, numerical computations in terms of principle stretches are expensive and not at all efficient for (explicit) dynamic computations.

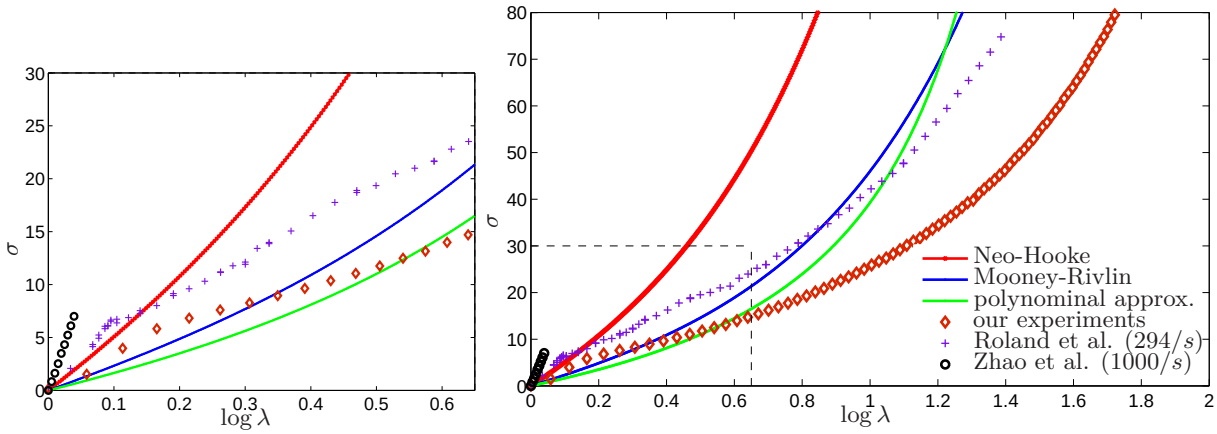

Figure 7: Approximated stress-strain curves of the elastic models for simulation of the Taylor anvil test; the left plot shows the inset marked on the right

A reduced slope of the stress-strain curve may be obtained via the second invariant, see Fig. 4. Whereas the first invariant has a clear physical meaning (measuring the stretch of a line element), the effect of the second invariant is less obvious. In uniaxial tension, models using the second invariant seem to be softer than the corresponding Neo-Hookean material with $\mu = \mu_1 + \mu_2$. However, this is misleading, in equibiaxial tension the Mooney-Rivlin type of materials are much stiffer, see Fig. 6. Picturing the second invariant as measure of surface element deformation this may be illustrated. For example, a volume preserving uniaxial stretching of a unit cube with $\lambda = 2$ leads to a 29% longer diagonal and $\approx 11\%$ more surface of the material element. An equibiaxial stretching with $\lambda = \sqrt{2}$, however, lengthens the diagonal of 19% and gives $\approx 14\%$ more surface to the material element. In this way, parameter μ_2 characterizing the resistance against 'surface extension' is weighted strongly. Such a material response can only be verified by experiments under multiaxial conditions. A pure shear test, as performed in Chakkarapani et al. (2006) is not sufficient, because a distinction between first and second invariant is not possible here, cf. Tab. 3. Models which employ high order terms of the second invariant, e.g. model (26-27), describe a form of strain stiffening which is hard to validate.

Summarizing we state that it may be tempting to fit the material parameter in a way that the curves of experimental data and model lay on top of each other. However, such fits pretend an accuracy which is usually not supported by different experimental setups, cf. El Sayed (2008); Xue et al. (2010). Moreover, no elastic model is able to map a strong initial but subsequently rapidly decaying stiffness. Wether such material data are artifacts of experiments on soft polymers or wether this softening is due to some kind of damage (comparable, e.g., to the Mullins effect of rubber), this is not to answer without additional experimental investigations under different conditions. Employing the classical models of hyperelasticity the material constants can only be adapted to the strain rage of interest in an averaging manner.

4 Numerical Example

In the following we present simulations of the Taylor anvil impact experiment, cf. Fig. 1. The experiments have been performed by Mock et al. at the Naval Surface Warfare Center, Dahlgren, VA, USA; using a $1/2 \times 1$ in. specimen of polyurea with an impact velocity of 246 m/s, cf. Reina (2010) for more information. The deformation of the specimen has been recorded and the monitored contour plots will be compared with the our numerical simulations here.

In consequence of the discussion above we model the specimen with the simplest possible material models, namely a Neo-Hookean (NH) and a Mooney-Rivlin (MR) model and, additionally, with a polynomial model. In order to consider the effect of strain stiffening observed by Roland et al. (2007) we state a model of the form:

$$W = \frac{\mu_1}{2}\big(I_1 - 3\big) + \frac{\mu_3}{6}\big(I_1 - 3\big)^3 \qquad \Rightarrow \qquad \boldsymbol{\sigma} = -p\boldsymbol{I} + \mu_1 \boldsymbol{B} + \mu_3 \big(I_1 - 3\big)^2 \boldsymbol{B} \tag{44}$$

The rate dependence is taken into account by the initial shear modulus, its calibration to the experimental data, however, is not straightforward. We may fit to the initial slope, to the full range of measurements

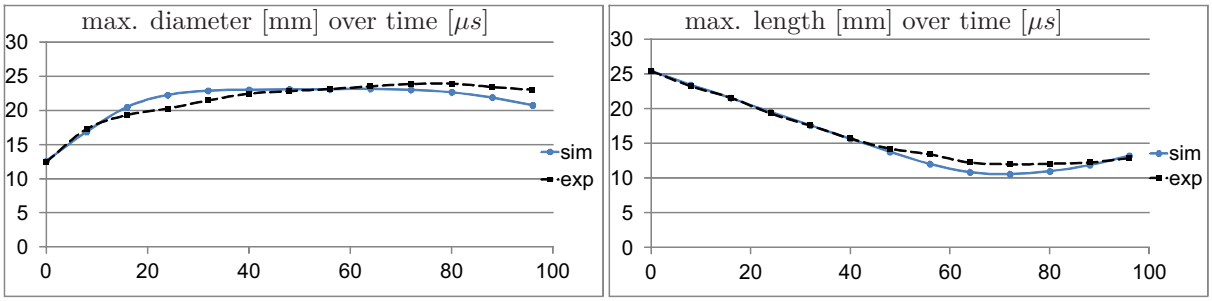

Figure 8: Comparison of the deformation during the experiment and a simulation using the Neo-Hookean model

or to the range of interest in our simulation. The first has been done with the Neo-Hookean model and $\mu = 16$ MPa which is still less than the value given by Knauss and Zhao (2007) for linear elasticity ($E = 69$ MPa/$\mu = 23$ MPa). For $\epsilon \leq 0.2$ ($\lambda = 1.25$) the fit gives a fair agreement, for larger straining it clearly deviates from the experimental curves. A good fit to a wider range of measurement gave model (44) with small values of μ_1 and μ_3. Clearly, for small straining it then underestimates the stiffness of the material, whereas for high straining it shows pronounced stiffening. We use $\mu_1 = 5.2$ MPa and $\mu_3 = 0.015$ MPa, which agrees reasonable well with the experimental data of Roland et al. (2007) at strain rates of 294/s (engineering strain rate of 573/s). A similar fit to the range of interest -the Taylor bar is compressed to half of its length- gives a Mooney-Rivlin model with $\mu_1 = 6$ MPa, $\mu_2 = 1.5$ MPa. Fig. 7 shows the corresponding stress strain curves together with some experimental results in two different scales.

Let us mention that the material parameters have been thoroughly adapted, and combinations of the above mentioned models, e.g., a softer Neo-Hookean model with $\mu = \mu_1 + \mu_2$ or a Mooney-Rivlin model with additional 3-rd order term as in (44), have been tested as well. The latter give comparable results, but we omit them here for clarity and compare the performance of the three different models in the Taylor anvil impact simulation instead.

The numerical simulation uses an explicit Newmark scheme. The spacial discretization is done with 800 hexahedral finite elements. The unilateral contact is assumed to be frictionless; the effect of friction has been studied but is negligible (Voll, 2009). To approximate incompressibility the volumetric part of the elastic energy is modeled by an elastic energy density $W = {}^{K}/_{2}(1 - J)^2$ with $K \approx 100\mu$. Figures 8-11 summarize the results.

From Fig. 8 and 9 we can see that all three models are appropriate to simulate the experiment. Not only the diameter and length fit well, also the shape of the deformation are adequately recreated. All the simulation results almost coincide during compression until $\approx 50\mu$s. In the softer polynomial model the deformation is somewhat larger than in the Mooney-Rivlin and Neo-Hookean models, see Fig. 9.

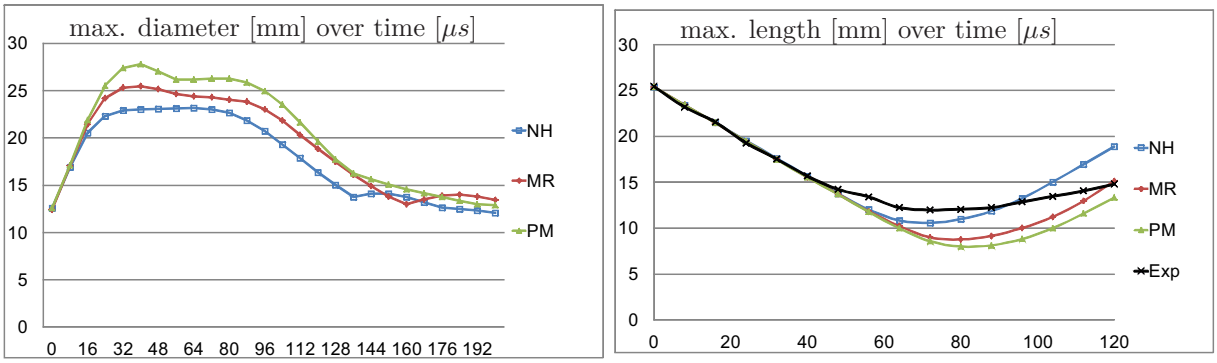

Figure 9: Deformation during simulation data for Neo-Hookean (NH), Mooney-Rivlin (MR) and polynomial model (PM)

The maximal compression is reached at 72μs, then follows the relaxation period, which now shows differences for the different models. The contours of the Mooney-Rivlin model in Fig. 10 and the polynomial model in Fig. 11 show a sidewards bulging and for the latter a stronger compression. Apparently the 3-rd order term in (44) does capture resistance against (fast) compression here. However, the overall deformation versus time is best matched by the Mooney-Rivlin model, as well as the relaxation of length, see Fig. 9.

Because all models are elastic the specimen later start to oscillate, i.e., to compress and relax periodically. This, of course, is not realistic but as we do not model any dissipation it is correct. Here an improvement can be achieved using a viscoelastic model and/or by including damaging effects, which, however, is beyond the scope of this paper. Therefore, regarding the fit to experimental data as well as the Taylor anvil test simulations, we recommend for dynamic elastic modeling of polyurea a Mooney-Rivlin material model with $\mu_1 = 6$ MPa, $\mu_2 = 1.5$ MPa.

4.1 Acknowledgements

The authors wish to thank *Voelkel Industrie Produkte GmbH (VIP)* in Munich for supplying us with samples of polyurea.

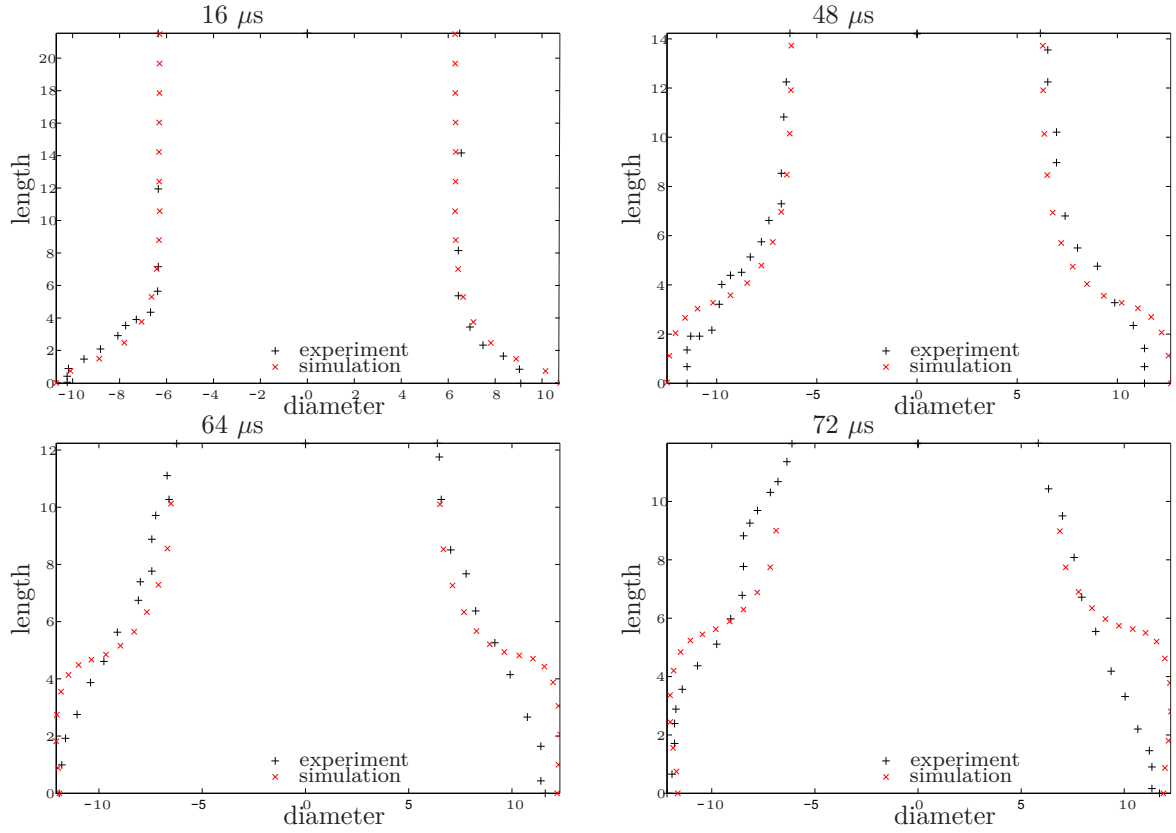

Figure 10: Comparison of the shape of the specimen in experiment and simulation using a Mooney-Rivlin model at 16μs, 48μs, 64μs and 72μs

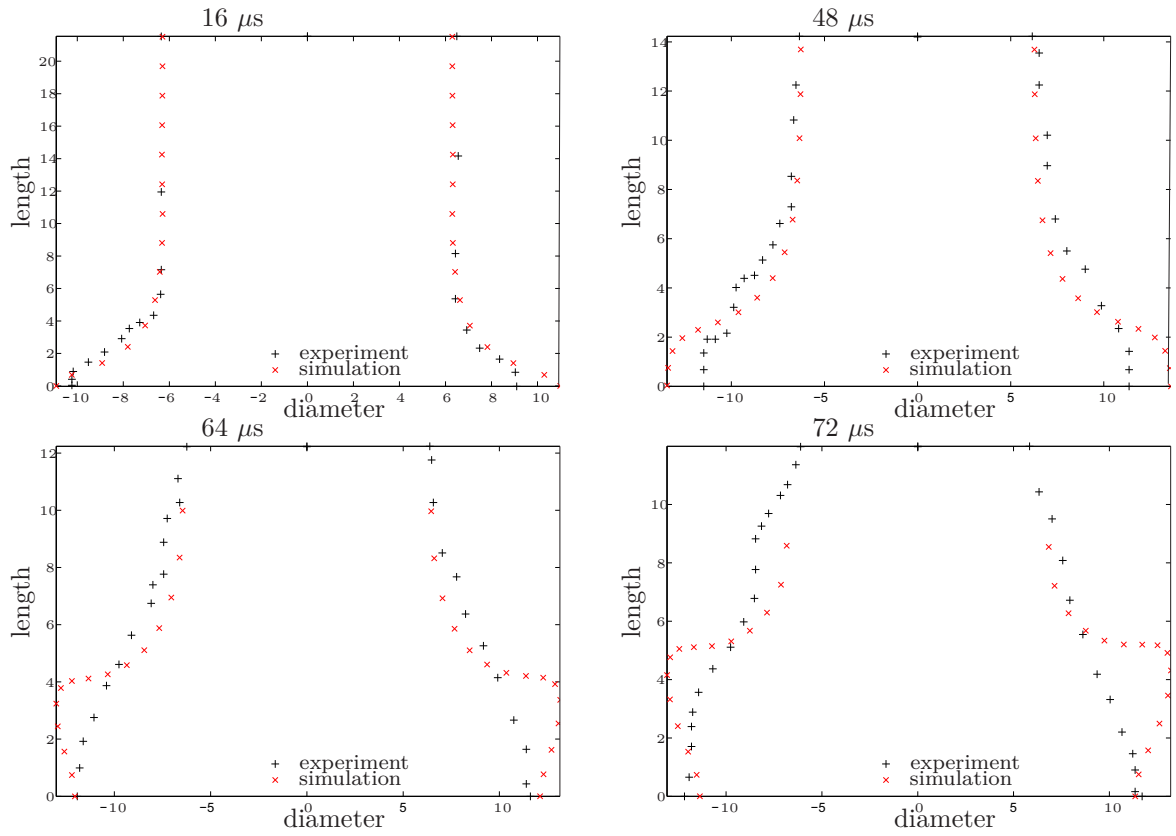

Figure 11: Comparison of the shape of the specimen in experiment and simulation using the polynomial model (44) at 16μs, 48μs, 64μs and 72μs

References

Amirkhizi, A. V.; Isaacs, J.; Mcgee, J.; Nemat-Nasser, S.: An experimentally-based viscoelastic constitutive model for polyurea, including pressure and temperature effects. *Philosophical Magazine*, 86, (2006), 5847–5866.

Arruda, E. M.; Boyce, M. C.: A three-dimensional constitutive model for the large stretch behavior of rubber elastic materials. *Journal Mech. Physics Solids*, 41, (1993), 389–412.

Ball, J. M.: Convexity conditions and existence theorems in nonlinear elasticity. *Archive for Rational Mechanics and Analysis*, 63, 4, (1976), 337–403.

Bilgili, E.: Restricting the hyperelastic models for elastomers based on some thermodynamical, mechanical, and empirical criteria. *Journal of Elastomers and Plastics*, 36, (2004), 159 – 175.

Chakkarapani, V.; Ravi-Chandar, K.; Liechti, K. M.: Characterization of multiaxial constitutive properties of rubbery polymers. *Journal of Engineering Materials and Technology*, 128, (2006), 489–494.

El Sayed, T.; Mock, W.; Mota, A.; Fraternali, F.; Ortiz, M.: Computational assessment of ballistic impact on a high strength structural steel/polyurea composite plate. *Computational Mechanics*, 43, (2009), 525–534.

El Sayed, T. M.: Constitutive models for polymers and soft biological tissues. PhD-Thesis, California Institute of Technology Pasadena (2008).

Fung, Y.: Elasticity of soft tissues in simple elongation. *American Journal of Physiology*, 213, (1967), 1532–1544.

Gent, A. N.: A new constitutive relation for rubber. *Rubber chemistry and technology*, 69, (1996), 59–61.

Hartmann, S.; Neff, P.: Polyconvexity of generalized polynomial-type hyperelastic strain energy functions for near-incompressibility. *International Journal of Solids and Structures*, 40, (2003), 2767–2791.

Hoss, L.; Marczak, R.: A new constitutive model for rubber-like materials. *Mecánica Computacional*, 29, (2010), 2759–2773.

Kilian, H.-G.: A molecular interpretation of the parameters of the van der Waals equation of state for real networks. *Polymer Bulletin*, 3, (1980), 151–158.

Kilian, H.-G.: Equation of state of real networks. *Polymer*, 22, 2, (1981), 209–217.

Knauss, W. G.; Zhao, J.: Improved relaxation time coverage in ramp-strain histories. *Mechanics of Time-Dependent Materials*, 11, (2007), 199–216.

Morrey, C. B.: *Multiple integrals in the calculus of variations*. Springer, Berlin (1966).

Ogden, R.: Large deformation isotropic elasticity – on the correlation of theory and experiment for incompressible rubberlike solids. *Proceedings of the Royal Society of London. A. Mathematical and Physical Sciences*, 326, 1567, (1972), 565–584.

Reina, C.: Multiscale modeling and simulation of damage by void nucleation and growth. PhD-Thesis, California Institute of Technology Pasadena (2010).

Rivlin, R.; Saunders, D.: Large elastic deformations of isotropic materials. VII. experiments on the deformation of rubber. *Philosophical Transactions of the Royal Society of London. Series A, Mathematical and Physical Sciences*, 243, (1951), 251–288.

Roland, C. M.; Twigg, J. N.; Vu, Y.; Mott, P. H.: High strain rate mechanical behavior of polyurea. *Polymer*, 48, (2007), 574–578.

Sarva, S. S.; Deschanel, S.; Boyce, M. C.; Chen, W.: Stressestrain behavior of a polyurea and a polyurethane from low to high strain rates. *Polymer*, 48, (2007), 2208–2213.

Tekalur, S. A.; Shukla, A.; Shivakumar, K.: Blast resistance of polyurea based layered composite materials. *Composite Structures*, 84, (2008), 271–281.

Treloar, L. R. G.: Stress-strain data for vulcanized rubber under various types of deformation. *Proceedings of the Faraday Society*, 40, (1944), 59–70.

Voll, L. B.: Numerische Untersuchung des Verhaltens von Polyurea bei schlagartiger Belastung. Diplomarbeit, Technische Universität Berlin (2009).

Xue, L.; Mock, W.; Belytschko, T.: Penetration of DH-36 steel plates with and without polyurea coating. *Mechanics of Materials*, 42, (2010), 981–1003.

Yeoh, O. H.: Some forms of the strain energy function for rubber. *Rubber chemistry and technology*, 66, (1996), 754–771.

Yi, J.; Boyce, M. C.; Lee, G. F.; Balizer, E.: Large deformation rate-dependent stress-strain behavior of polyurea and polyurethanes. *Polymer*, 47, (2006), 319–329.

Zhao, J.; Knauss, W.; Ravichandran, G.: Applicability of the time–temperature superposition principle in modeling dynamic response of a polyurea. *Mechanics of Time-Dependent Materials*, 11, (2007), 289–308.

Address: Universität Siegen, Fakultät IV, Dept. Maschinenbau, Lehrstuhl für Festkörpermechanik, Paul-Bonatz-Str. 9-11, D-57076 Siegen, Germany
email: `thomas.reppel | tim.dally | kerstin.weinberg@uni-siegen.de`